Climate-driven oscillation of phosphorus and iron limitation in the North Pacific Subtropical Gyre

Ricardo M. Letelier[a,1], Karin M. Björkman[b,c], Matthew J. Church[d], Douglas S. Hamilton[e], Natalie M. Mahowald[e], Rachel A. Scanza[e,2], Niklas Schneider[c,f], Angelicque E. White[b,c], and David M. Karl[b,c,1]

[a]College of Earth, Ocean, and Atmospheric Sciences, Oregon State University, Corvallis, OR 97331; [b]Daniel K. Inouye Center for Microbial Oceanography: Research and Education, University of Hawai'i at Manoa, Honolulu, HI 96822; [c]Department of Oceanography, University of Hawai'i at Manoa, Honolulu, HI 96822; [d]Flathead Lake Biological Station, University of Montana, Polson, MT 59860; [e]Department of Earth and Atmospheric Sciences, Cornell University, Ithaca, NY 14850; and [f]International Pacific Research Center, University of Hawai'i at Manoa, Honolulu, HI 96822

Contributed by David M. Karl, May 1, 2019 (sent for review January 15, 2019; reviewed by Philip W. Boyd and Thomas S. Weber)

The supply of nutrients is a fundamental regulator of ocean productivity and carbon sequestration. Nutrient sources, sinks, residence times, and elemental ratios vary over broad scales, including those resulting from climate-driven changes in upper water column stratification, advection, and the deposition of atmospheric dust. These changes can alter the proximate elemental control of ecosystem productivity with cascading ecological effects and impacts on carbon sequestration. Here, we report multidecadal observations revealing that the ecosystem in the eastern region of the North Pacific Subtropical Gyre (NPSG) oscillates on subdecadal scales between inorganic phosphorus (P_i) sufficiency and limitation, when P_i concentration in surface waters decreases below 50–60 nmol·kg^{-1}. In situ observations and model simulations suggest that sea-level pressure changes over the northwest Pacific may induce basin-scale variations in the atmospheric transport and deposition of Asian dust-associated iron (Fe), causing the eastern portion of the NPSG ecosystem to shift between states of Fe and P_i limitation. Our results highlight the critical need to include both atmospheric and ocean circulation variability when modeling the response of open ocean pelagic ecosystems under future climate change scenarios.

pelagic ecosystem | phosphorus limitation | atmospheric iron deposition | Pacific Decadal Oscillation | climate

The vast open ocean subtropical gyres (covering ∼40% of the Earth's surface) are characterized by well-stratified surface waters containing vanishingly low concentrations of inorganic nutrients. The optical clarity of these pelagic environments allows sunlight to penetrate to great depths, often supporting photosynthetic activity well below 100 m (1). In addition, an almost permanent stratification of the upper water column leads to the chronic biological depletion of nutrients from these well-lit surface layers, increasing the difficulty of replacing them by vertical diffusion and through the mixing of nutrient-rich deep waters (2).

While the primary replenishment mechanism in surface waters for macronutrients, such as nitrogen (N) and phosphorus (P), is through the diffusion and vertical mixing of deep nutrient-rich waters and/or lateral advection (3), the input of micronutrients, especially iron (Fe), occurs mainly via atmospheric dust deposition (4, 5). Inputs of Fe from below the euphotic zone are negligible as the low Fe solubility (fraction of total Fe that is soluble, of which a portion is considered "bioavailable") in well-oxygenated deep waters generates a deficiency in Fe relative to other nutrients (6). In addition, N can be introduced into the pelagic food web through nitrogen (N_2) fixation, a process carried out by specialized microorganisms termed diazotrophs, during which some of the abundant N_2 dissolved in seawater is reduced to ammonia (7). Consequently, diazotrophic activity is ultimately limited by the availability of other nutrients, such as P and Fe (8, 9). In this context, large spatial and temporal variability in the residual inorganic phosphorus (P_i) concentration in oligotrophic surface waters reflects the capacity of the microbial assemblages to deplete this macronutrient (10, 11). In addition, although different species display distinct strategies to cope with nutrient limitation (12, 13), the elemental ratio of suspended particulate matter in oligotrophic pelagic environments is confined to a narrow range (14, 15), suggesting limited plasticity in the overall stoichiometry of the microbial assemblage's biological demand. As a result, the observed variability in residual nutrients denotes the large-scale uncoupling of nutrient supply stoichiometry relative to the microbial nutrient consumption ratio in these otherwise physically stable ecosystems (10).

The uncoupling of the stoichiometry in nutrient supply is clearly observed at global scales. While the summertime conditions of the North Atlantic Subtropical Gyre display vanishing small concentrations of P_i (<10 nM) in response to sustained atmospheric deposition of Fe-rich dust from the Sahara (16, 17), the South Pacific is characterized by persistently high P_i concentrations (∼100 nM) and low dust deposition rates (18, 19). Furthermore, model-derived latitudinal and seasonal gradients in dust deposition have been used to explain patterns in N_2 fixation

Significance

Characterizing the mechanisms driving spatial and temporal changes in the stoichiometry of nutrient supply is crucial to understand the controls of an ecosystem's carrying capacity and productivity. In marine oligotrophic regions, small changes in the ocean and atmospheric nutrient input ratio can shift the nature of the limiting nutrient. The present study documents such a shift at interannual scales between periods of phosphorus limitation and sufficiency in the North Pacific Subtropical Gyre. These shifts appear to be driven by interannual variations in the transport of iron-rich Asian dust across the North Pacific resulting from basin-scale changes in atmospheric pressure gradients, as reflected by the Pacific Decadal Oscillation index, causing the ecosystem to oscillate between phosphorus and iron limitation.

Author contributions: R.M.L. and D.M.K. designed research; R.M.L., K.M.B., M.J.C., A.E.W., and D.M.K. performed research; R.M.L. and D.M.K. contributed new reagents/analytic tools; R.M.L., K.M.B., M.J.C., D.S.H., N.M.M., R.A.S., N.S., A.E.W., and D.M.K. analyzed data; R.M.L., N.S., A.E.W., and D.M.K. wrote the paper; and D.M.K. provided primary funding for the research.

Reviewers: P.W.B., University of Tasmania; and T.S.W., University of Rochester.

The authors declare no conflict of interest.

[1]To whom correspondence may be addressed. Email: letelier@oregonstate.edu or dkarl@hawaii.edu.

[2]Present address: Atmospheric Sciences and Global Change Division, Pacific Northwest National Laboratory, Richland, WA 99354.

This article contains supporting information online at www.pnas.org/lookup/suppl/doi:10.1073/pnas.1900789116/-/DCSupplemental.

Published online June 10, 2019.

and residual P_i concentrations within ocean basins (10, 20). Hence, despite their similarities in terms of vertical stratification, light regime, and biological carrying capacity, subtropical gyres encounter distinct proximate elemental controls of ecosystem productivity and export caused by an uncoupling in the source of nutrients, leading to spatial and temporal variability in the supply ratio of these resources (21).

Other processes also contribute to the observed variability in upper water column P_i concentrations. In the eastern region of the North Pacific Subtropical Gyre (NPSG), as recorded at Station ALOHA (22°45′N, 158°00′W), significant subdecadal oscillations in P_i surface concentrations (22) have been linked to basin-scale climate shifts via two distinct mechanisms. The first mechanism relates to an enhancement of upper ocean water column stratification leading to a decrease in nitrate (NO_3^-) and P_i input into the upper layers through the diffusion and mixing of nutrient-rich waters from below the euphotic zone. This enhanced stratification selects for a pelagic microbial ecosystem in which N_2 fixation plays an increasing role, shifting the reliance on new N from NO_3^- to N_2 and driving the ecosystem into a state of P_i limitation (22, 23). A second mechanism, not necessarily independent from that of water column stratification, is the shift in source waters reaching Station ALOHA (24), a process that could alter both the microbial assemblage and chemistry of waters advected into this sampling region.

Ongoing observations at Station ALOHA since 1988 by the Hawaii Ocean Time-series (HOT) program have provided over three decades of relatively high frequency (near monthly) physical and biogeochemical data from which low-frequency variability can be characterized and quantified (25). Over this period, the two dominant climate modes describing oceanic variability in the eastern region of the NPSG, the North Pacific Gyre Oscillation (NPGO) and the Pacific Decadal Oscillation (PDO), have displayed significant fluctuations (26), allowing us to assess the relationship between changes in physical and biogeochemical conditions at Station ALOHA and basin-scale processes represented by these climate indices.

Evidence of Variability in Microbial Metabolic P_i Limitation

Based on P_i uptake kinetic experiments conducted at Station ALOHA between 2002 and 2010, Björkman et al. (27) observed that the mean P_i concentration (K_m) required to achieve the half-maximum uptake rate [$V_{max(0.5)}$] in whole-water microbial communities was 28 ± 5 nmol·kg^{-1} (n = 9). Using the doubling of K_m as a conservative estimate of the minimum concentration required to saturate P_i uptake kinetics, we derive a P_i limitation threshold of ∼50–60 nmol·kg^{-1} for this pelagic microbial assemblage (Fig. 1).

In addition, studies assessing the role of P_i in limiting N_2 fixation rates in this oligotrophic environment have yielded variable results. While in July to August 2008 Watkins-Brandt et al. (28) found that N_2 fixation rates in the mixed layer by the filamentous cyanobacteria *Trichodesmium* spp. were enhanced following the addition of P_i, Gradoville et al. (29) observed no such response in March 2011. Similarly, earlier work by Grabowski et al. (30) based on whole-water incubations suggested that N_2 fixation rates at Station ALOHA increased following P_i additions only in some field experiments. However, when reevaluating Grabowski's experimental results (30) as a function of in situ P_i conditions, we observe that P_i additions enhanced N_2 fixation rates only when ambient P_i concentrations fell below 50 nmol·kg^{-1} (Fig. 1). Despite the limited sample size, this observation is consistent with the results by Watkins-Brandt et al. (28) and Gradoville et al. (29), who reported P_i background concentrations of <40 and >70 nmol·kg^{-1}, respectively, when assessing the effect of P_i amendment on N_2 fixation rates. Moreover, although P_i represents less than 20% of the total dissolved P pool in these oligotrophic ecosystems (28, 31), the observed enhancement of N_2 fixation following P_i additions

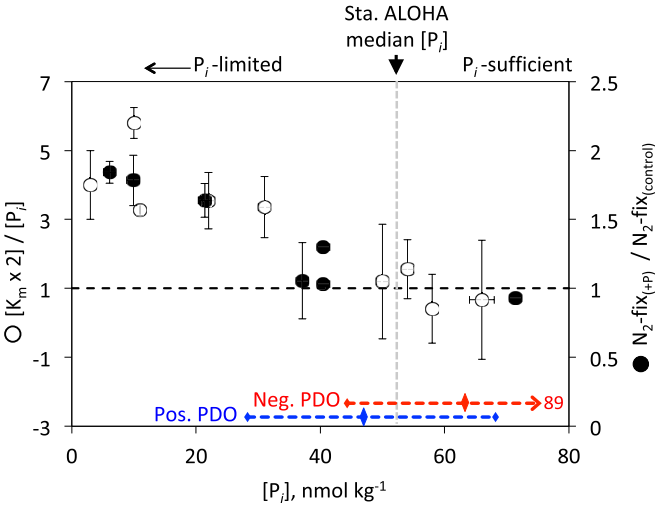

Fig. 1. Threshold concentrations for P_i limitation: The solid circles represent the relative enhancement of N_2 fixation rates in mixed-layer samples following P_i addition, plotted as a function of ambient P_i concentration. The open circles are estimates of the minimum concentration required to saturate P_i uptake kinetics of the microbial assemblage—calculated as twice [K_m] (i.e., the P_i concentration required to support one-half the maximum uptake rate derived from the Michaelis–Menten equation)—relative to the ambient P_i concentration, plotted as a function of in situ P_i concentration [data from Grabowski et al. (30) and Björkman et al. (27), respectively]. The observed median P_i concentration in the upper euphotic zone (0–45 m) for the period 1989–2015 is marked by the vertical dashed line; the 75th percentile range and median P_i concentration observed during positive and negative PDO phases are displayed in blue and red, respectively.

when background concentrations drop below 50 nmol·kg^{-1} suggests that other forms of P, such as some dissolved organic compounds known to be metabolized by specific marine diazotrophs (32), may not be readily available to most diazotrophs or may only be available to organisms displaying low N_2 fixation rates and to populations that are unable to fix N_2.

Over the past 3 decades the median P_i concentration observed in the upper euphotic zone at Station ALOHA (0- to 45-m depth, defined by the nominal 3 upper sampling depths of the HOT program) was 53 nmol·kg^{-1} (SEM = 2.2 nmol·kg^{-1}; n = 261), a value close to the critical concentration at which we predict P_i becomes limiting to N_2 fixation and whole-water microbial assemblages in this oceanic region. Since 1989, the HOT program has recorded subdecadal oscillations between phases of predominantly low P_i concentrations (<60 nmol·kg^{-1}) and phases with P_i concentrations exceeding 70 nmol·kg^{-1} (Fig. 2). Furthermore, when looking at the long-term variability in the context of North Pacific climate indices, the 0- to 45-m median (±SEM) P_i concentration during positive PDO periods is 47 ± 4.1 nmol·kg^{-1} (n = 159), rising to 64 ± 3.6 nmol·kg^{-1} (n = 102) for negative PDO periods (Figs. 1 and 2 and *SI Appendix*, Fig. S1), suggesting that microbial assemblages may oscillate between P-limitation and P-sufficiency as the PDO shifts between positive and negative phases (33).

Climate Forcing in the Eastern Region of the NPSG

Both the PDO and NPGO climate indices represent the upper ocean response to North Pacific basin-scale changes in atmospheric forcing. The PDO is a well-documented mode of climate variability characterized by the principal component of sea surface temperature anomalies (SSTAs) (34). This variability has been linked to anomalous variations in atmospheric sea-level pressure (SLP) due, in part, to changes in the strength and position of the North Pacific Ocean low-pressure feature referred to as the

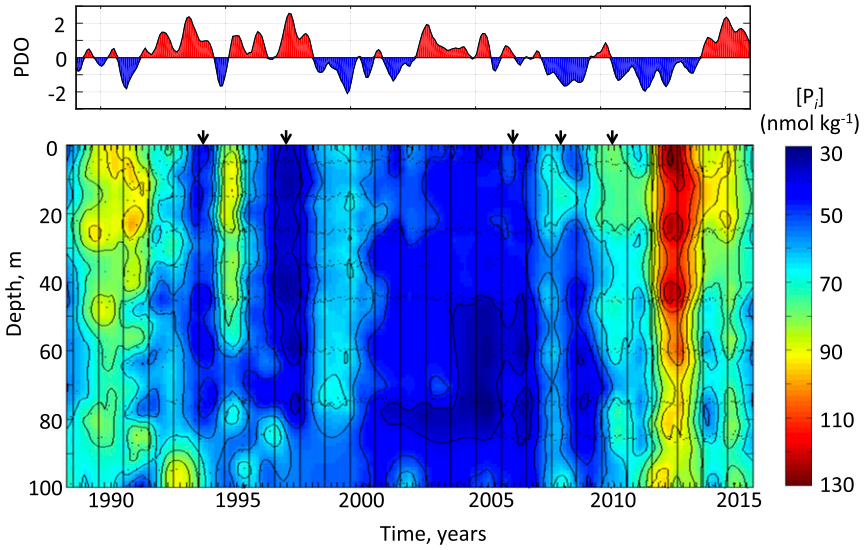

Fig. 2. Time series of (*Upper*) the Pacific Decadal Oscillation (PDO) and (*Lower*) P_i concentration in the upper water column (0–100 m) at Station ALOHA. The arrows in the *Lower* panel mark periods following large springtime atmospheric Fe concentration values (mean monthly concentration >40 ng·m^{-3} for particle size fraction <2.5 μm) as recorded at the Mauna Loa Observatory.

Aleutian Low (35); while negative phases of the PDO are associated with a weakening of the Aleutian Low, its strengthening contributes to positive phases of the PDO. In the eastern region of the NPSG, a positive PDO is reflected in both low sea surface height anomalies (SSHAs) and low SSTAs, leading to a deepening of winter mixed-layer depth (36).

In addition, the NPGO, defined as the second leading principal component of SSHAs over the northeastern region of the Pacific Ocean (26), closely tracks the second leading principal component of SSTAs. This climate index is the oceanographic expression of the North Pacific Oscillation (NPO), which is associated with the variability in SLP between Hawaii and Alaska (37), also reflecting changes in the strength of the Aleutian Low (38). Furthermore, the NPGO captures changes in the strength of gyre circulation, particularly the Kuroshio–Oyashio Extension (KOE) (39) and the North Pacific Current (NPC) (40).

Both the PDO and NPGO indices are driven by shifts in basin-scale atmospheric pressure gradients and ocean circulation. These shifts affect the stratification of the upper water column as well as the large-scale oceanic and atmospheric patterns in advection. Some of these effects can be observed at Station ALOHA where seasonally detrended mixed-layer density and upper water column stratification, defined as the difference in density between the mixed-layer and 150-m depth horizon, are significantly correlated to the NPGO and PDO indices (Table 1 and *SI Appendix*, Fig. S2). However, the advection of surface water, as derived from diagnostic models of ocean near-surface circulation (Ocean Surface Current Analysis Real-Time) (41), or through the drift of sediment traps deployed over a 48- to 72-h period at Station ALOHA during each approximately monthly cruise, do not display distinct patterns associated with changes in North Pacific climate indices (*SI Appendix*, Fig. S3).

Although water column stratification at Station ALOHA appears to respond to changes in atmospheric and oceanographic forcing captured by both the PDO and NPGO, the variability in 0- to 45-m P_i concentrations does not correlate with interannual oscillations in the local mixed-layer density anomaly or upper water column stratification (Table 1 and *SI Appendix*, Fig. S2). Nevertheless, we observe a significant negative correlation between P_i and the PDO index with a 4-mo lag period (PDO leading; one-way ANOVA, $P < 0.001$; Fig. 2 and *SI Appendix*, Fig. S1 and Table S1), suggesting that the observed variability in P_i and the PDO results from a common atmospheric forcing; the temporal lag may result from both the physical and biological timescale response of the surface ocean to changes in basin-scale atmospheric forcing (42).

Ruling Out Potential Hawaiian Island Sources of P_i and Fe Interannual Variability

Kīlauea, an active volcano located on the Island of Hawaii ∼400 km southeast of Station ALOHA, has been erupting almost continuously since 1983 (43). The resulting volcanic plume represents a potentially significant source of P_i and Fe to the marine environment (44–46). However, neither remote sensing-based plume dispersion observations and models (47), nor wind patterns recorded by National Data Buoy Center Buoys 51001 and 51101

Table 1. Cross-correlation coefficient for seasonally detrended mixed-layer properties, North Pacific climate indices, and atmospheric Fe concentration

Environmental parameter	Mauna Loa aerosol Fe concentration	Mixed-layer density	Mixed-layer to 150-m density gradient	NPGO index	PDO index
Mean 0- to 45-m depth P_i concentration	*−0.183 (0.0)*	0.03 (0.0)	0.00 (0.0)	0.11 (+0.5)	**−0.36 (+0.4)**
Model-derived atmospheric Fe concentration	**0.45 (0.0)**			**−0.48 (0.0)**	**0.47 (0.0)**
Mixed-layer density			**−0.82 (0.0)**	**0.55 (−0.9)**	**−0.38 (−0.2)**

Bold values indicate $P < 0.01$; italic value indicates $P < 0.05$. Temporal lag in years is displayed in parentheses.

(24°27.17′N 162°00′W and 24°21.47′N 162°03.5′W, respectively) display significant shifts in velocity and direction between PDO phases (*SI Appendix*, Fig. S4).

In addition, recent studies on the temporal distribution of dissolved Nd and Ra isotopes at Station ALOHA suggest a lithogenic input from the Hawaiian Islands into the surface waters of Station ALOHA during winter months (48). However, as for the wind fields, the observed velocity and direction of ocean surface currents surrounding Station ALOHA remain consistent between PDO phases (*SI Appendix*, Fig. S3). This consistency in wind and ocean currents suggests that regional changes in advective patterns around the Hawaiian Islands cannot explain the observed subdecadal variability in P_i concentrations at Station ALOHA.

Assessing the Link Between Climate Forcing and Station ALOHA P_i Concentrations

Basin-scale patterns of temporal variability in SLP reflect changes in atmospheric forcing, including winds, storms, the passage of fronts, as well as atmospherically induced ocean mixing and advection. For this reason, it is possible that the interannual oscillations in P_i recorded at Station ALOHA may be driven by large-scale SLP changes observed in remote regions of the North Pacific basin. This hypothesis can be tested through a spatially resolved first-order autoregressive model (AR–1) analysis of P_i as a function of SLP:

$$\overline{P_i}^{j+1} = \alpha^* \overline{P_i}^{j} + \gamma \overline{SLP}^{j}, \quad [1]$$

where $\overline{P_i}^{j+1}$ denotes July to June annual averages with the superscript corresponding to the year counter, $\alpha^* = 1 - \alpha\,\Delta t$ accounts for the damping timescale α; α^* and γ are determined by least-square fit of P_i using a time step Δt of 1 y (35, 49).

When forced by SLP anomalies centered on 40°N, 160°E in the Northwest Pacific, Eq. **1** skillfully captures annually averaged P_i observed in situ at Station ALOHA (Fig. 3). The best-fit value of $\gamma = 13.67$ implies a positive relationship between atmospheric processes captured by the Northwest Pacific SLP index and Station ALOHA P_i anomalies. The best-fit damping timescale ($\alpha^{-1} \sim 2$ y; *SI Appendix*, Fig. S5) suggests upper ocean tracer anomalies that are diminished primarily by ocean processes. Using the same AR–1 analytical approach, Schneider and Cornuelle (35) found that the correlation between the PDO index and SLP has a very similar basin-scale spatial distribution to that observed for Station ALOHA P_i versus SLP, with a maximum ($r > 0.8$) in the Northwest Pacific, colocated with the maximum observed in our AR–1 analysis between Station ALOHA P_i and SLP. This result supports our hypothesis that the significant correlation between the PDO index and Station ALOHA 0- to 45-m P_i concentration stems from a response to the same atmospheric forcing.

Interannual Basin-Scale Patterns on Fe Dust Deposition

Dust deposition is an important source of nutrients into the open ocean, including the NPSG, especially for Fe. In this context, several studies have suggested that changes in the position and strength of the Aleutian Low over the Northwest Pacific may affect the source and spatial patterns of Asian dust transport across the North Pacific (50–52). We hypothesize that these changes, driven by the interannual SLP variability in the western region of the North Pacific, can affect the overall supply and spatial distribution of atmospheric Fe-rich dust over the North Pacific at interannual to decadal timescales. While the Fe:P_i stoichiometry of the atmospheric dust reaching Station ALOHA is two orders of magnitude higher than that observed in the microbial biomass, the waters at the base of the euphotic zone (200 m) are significantly depleted in Fe (Table 2). Hence,

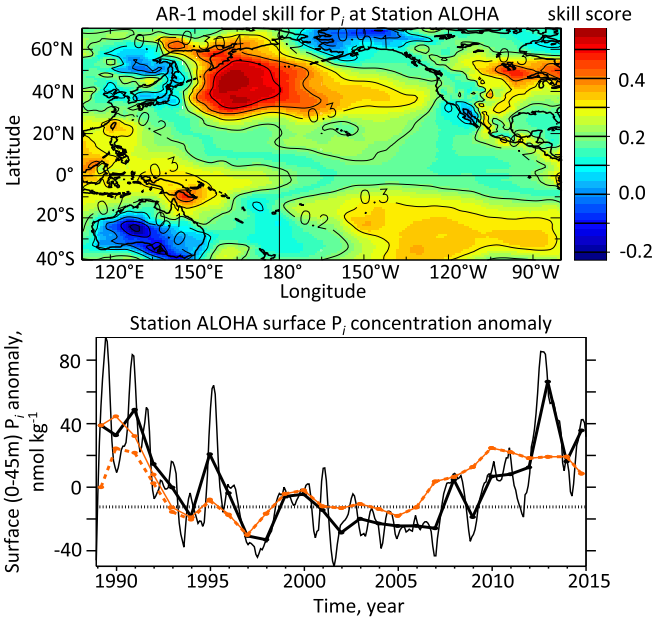

Fig. 3. (*Upper*) Spatial distribution of skill score as a function of local sea-level pressure (SLP) forcing time series for the reconstruction of annual averaged P_i at Station ALOHA using Eq. **1**. (*Lower*) Observed monthly anomalies of surface (0–45 m) P_i at Station ALOHA (thin black line) and July to June annual averages (thick black line). Reconstruction of annual P_i averages based on Eq. **1** and using SLP anomalies averaged over the area Northwest Pacific region where the skill score is >0.55 as the atmospheric forcing index, setting initial condition as 0 (dashed red line) and using initial observed condition (solid red line). The horizontal dotted line corresponds to the −12.4 nmol·kg^{-1} horizon and represents the anomaly required for annual P_i average to fall below the 50 nmol·kg^{-1} P_i-limitation threshold, the mean annual Pi average for the study period being 62.4 nmol·kg^{-1}.

changes in atmospheric dust transport and deposition can cause the pelagic ecosystem at Station ALOHA to oscillate between periods of P_i limitation, when Fe-dust deposition in the region is enhanced, and periods of P_i sufficiency, when dust-associated Fe supply decreases and Fe becomes the proximal limiting resource of microbial ecosystem productivity and export.

The predominant origins of Fe aerosol reaching the North Pacific's central and eastern regions are the soils of the arid and semiarid regions of China and Mongolia in Central Asia (50, 51). Model-based analyses also identify a secondary, smaller, continental source of Fe bearing aerosols generated through wildfires and anthropogenic combustion activities (52). However, the relative contribution of combustion sources decreases significantly with distance from the Asian coastline (53). Results from the Northern Aerosol Regional Climate Model and the reanalysis meteorology from the National Centers for Environmental Prediction suggest that the source of atmospheric dust from Asia shifts in response to climate forcing, displaying a significant correlation between the PDO (among other climate indices) and sources from Mongolia and central China (54). In addition, the position and strength of atmospheric flows carrying dust over the North Pacific, predominantly the jet stream, are also affected by changes in the position and strength of the Aleutian Low (39), which can potentially contribute to significant shifts in spatial patterns of Fe deposition over the NPSG.

Evidence of Interannual Variability in Fe Dust Deposition at Station ALOHA

Time-series records of labile Fe plus total dissolvable Fe (TDFe) (i.e., the soluble plus the acid labile particle Fe fraction) in the surface layers of the water column at Station ALOHA have been

Table 2. Iron (Fe) to phosphorus (P) stoichiometry in the nutrient supply terms, phytoplankton resident taxa, and particulate suspended matter, representative of Station ALOHA

Elemental source/pool	P	Fe	Fe:P, mol·mol^{-1}	Refs.
Water at the base of the euphotic zone as proxy for oceanic Fe and P_i supply, μmol·kg^{-1}				
200-m depth horizon	0.2	0.46 10^{-3}	0.002	77
	0.4*	0.76 10^{-3}	0.002	78
Atmospheric dust				
Concentration, nmol·m^{-3}	0.08	0.1	1.25	79
	Mean: 0.10†	0.35	0.7†	59
	Range: 0–15	0–2.7		
Deposition, μmol·m^{-2}·d^{-1}	0.02‡	0.02‡	1.0	64
	0.04§	0.24§	6.0	11
Cellular composition, mmol·mol^{-1} C				
Cyanobacteria				
Synechococcus	7.41	0.031	0.004	80, 81
	25.1–28.1	0.009–0.158	0.003–0.006	82
Prochlorococcus MED4	8.26	0.043	0.005	80, 83
Diatoms				
Thalassiosira weissflogii CCMP1336	10.31	0.0334	0.003	84
Diazotrophs				
Crocosphaera watsonii WH8501	7.7–9.9	0.027–0.18	0.003–0.023	85
Trichodesmium erythraeum IMS101	Mean: 5.41	0.035	0.006	86
and natural assemblages	Range: 3.2–12.7	0.018–0.078	0.002–0.015	
Trichodesmium spp. (nat. assemblages)	1.39–2.12	0.014–0.020	0.022–0.039	87
Suspended particulate matter, μmol·g^{-1}				
	227¶	1.01¶	0.004¶	88
	280	1.37	0.005	89
	260	1.3	0.005	90
			0.002–0.008#	91

*P_i concentration from the HOT cruise in which the Fe concentration was determined.
†Excluding P_i concentration values below detection limit.
‡Model-derived.
§Northwest Pacific Subtropical Gyre observations.
¶Northeast Atlantic observations.
#Equatorial Pacific for size fraction >3 μm.

intermittent and do not allow for a rigorous quantitative analysis of the long-term interannual variability of Fe in the context of shifts in climate indices (55). Nevertheless, at seasonal scales, TDFe concentrations follow a similar pattern as that observed in dust storm events over Asia, with maxima in spring or early summer and minimum values observed during late summer and autumn (56). In a detailed analysis of the seasonal and interannual TDFe concentration variability, Fitzsimmons et al. (55) observed that the intraannual variability was as large as that observed at interannual scales, suggesting that the residence time of TDFe in the upper ocean cannot be longer than a few months since the maximum seasonal concentrations observed in spring (May) appear to be depleted by late summer (October). In addition, as a result of their intensive daily sampling during field campaigns in the region near Station ALOHA, these authors were able to document a sudden increase in Fe between August 8th and 12th of 2012 that may have been caused by the upwelling associated with the passage of a cyclonic eddy just north of the sampling site. Although this and other observations (57) highlight the importance of stochastic events in modulating short-term availability of Fe at Station ALOHA, a deep-water upwelling event will result in an increase in P_i, leading to a potential surplus of P_i relative to Fe (58).

Alternatively, a long-term time-series aerosol record collected at the Mauna Loa Observatory between 1988 and 2011 provides field data to assess potential seasonal and interannual variability in atmospheric Fe availability in the vicinity of Station ALOHA (59). Based on the aerosol Fe time series (*SI Appendix*, Fig. S6), we observe that most years with extremely low late-summer P_i concentrations recorded in the upper euphotic zone at Station ALOHA (e.g., 1994, 1997, and 2006; Fig. 2) correspond to years in which the Mauna Loa record displays enhanced spring and early summer aerosol Fe values relative to the previous year. Nevertheless, there are some years with consistently low P_i (e.g., 2003 and 2004) that do not see a concomitant enhancement in atmospheric Fe concentrations, suggesting that the Mauna Loa record may not fully reflect the dynamics of atmospheric dust deposition in the waters sampled at Station ALOHA (i.e., the Mauna Loa Observatory is located at an altitude of 3,339 m and ~400 km southeast of Station ALOHA; *SI Appendix*, Figs. S6 and S7). Additional processes, such as the enhanced stratification recorded between 2002 and 2005 (Fig. 5 and *SI Appendix*, Fig. S3*C*), can further contribute to the observed variability in P_i. Still, we find a weak but significant negative correlation between the seasonally detrended Mauna Loa atmospheric Fe record and that of the mean 0- to 45-m P_i concentration at Station ALOHA (Table 1).

Another approach to assess the long-term climate-driven patterns of variability in atmospheric dust Fe availability over the North Pacific may be found in the implementation of the Community Atmospheric Model, version 4 (CAM4), embedded within the Community Earth System Model (CESM) (60). The model is forced with meteorology from the Modern-Era Retrospective Analysis for Research and Applications (MERRA) reanalysis-based simulations. It incorporates an intermediate complexity soluble Fe scheme that includes prognostic dust generation with soil mineralogy differences, combustion iron sources, as well as the transport, atmospheric processing, and deposition of dust, Fe,

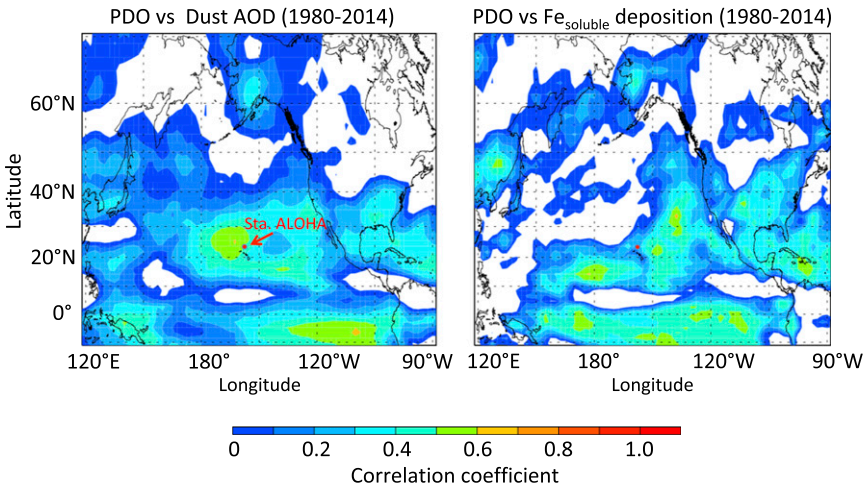

Fig. 4. Spatial distribution of the correlation coefficient for annual PDO index versus model run results of aerosol optical depth (AOD) attributed to dust (*Left*) and atmospheric soluble Fe deposition (*Right*) for the period 1980–2014. A solid red circle marks the location of Station ALOHA.

and soluble Fe (61). The model has been extensively compared with in situ observations and shown to capture much of the observed spatial and temporal variability (62), including that derived from the Mauna Loa time-series record (Table 1 and *SI Appendix*, Fig. S6).

Model outputs for the period 1980–2014 yield a positive correlation between PDO and Fe concentration (Table 1), aerosol optical depth, and Fe deposition (Fig. 4 and *SI Appendix*, Fig. S1) in the southeastern quadrant of the NPSG, confirming an overall enhancement of dust transport and Fe availability during positive PDO phases in the region surrounding Station ALOHA. A significant enhancement in atmospheric Fe deposition during positive PDO phases (9.8 ± 0.6 μmol Fe·m^{-2}·y^{-1} versus 6.2 ± 0.7 μmol Fe·m^{-2}·y^{-1} during negative PDO phases) and the concomitant decrease in sea surface P_i concentrations (*SI Appendix*, Table S1 and Fig. S1), support our hypothesis that climate-driven changes in Asian dust transport and atmospheric Fe deposition across the North Pacific, whose main source is mineral dust at this location (50, 55), may contribute significantly to interannual oscillation between P_i-sufficiency and limitation observed in microbial metabolic activity at Station ALOHA. Furthermore, our results are consistent with the model predictions of Ward et al. (10), who used global observations and a resource ratio framework to model competition between diazotrophs and nondiazotrophs; their modeling-based analysis suggests that oligotrophic pelagic ecosystems supporting diazotrophy shift from surplus P_i to P_i-deficiency when soluble Fe deposition rates exceed ~10 μmol Fe·m^{-2}·y^{-1}.

The Biogeochemical Coupling of Fe and P_i at Station ALOHA

Using the molar elemental stoichiometry of atmospheric and oceanic Fe:P_i at Station ALOHA (~0.7–1:1 and 0.002:1, respectively; Table 2) as end members of a mixing curve, we can derive a first-order approximation of the relative contribution needed to support a pelagic microbial assemblage with a specific

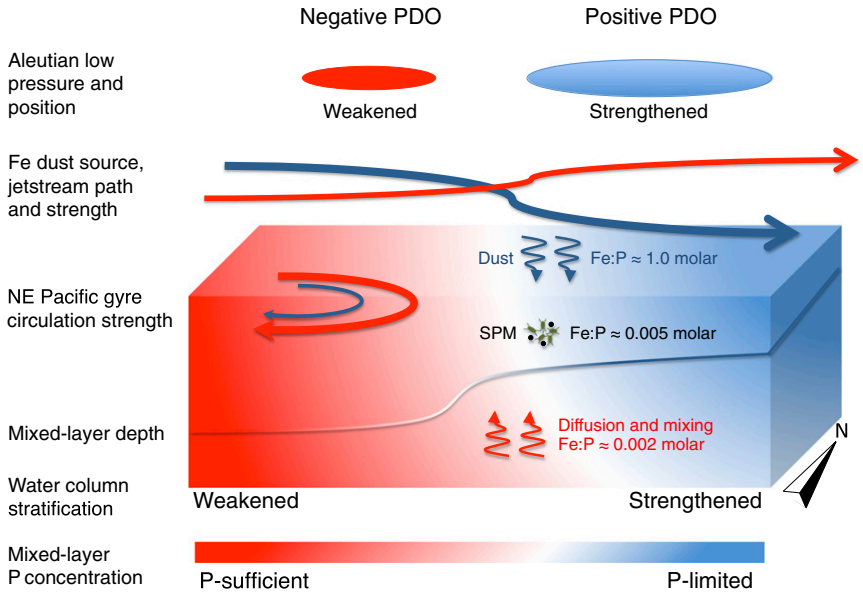

Fig. 5. Schematic diagram displaying the potential effects of climate-driven shifts in basin-scale atmospheric pressure gradients leading to the observed interannual variability in mixed-layer inorganic P concentration at Station ALOHA (red, P_i enhancement; blue, P_i depletion; SPM, suspended particulate matter).

Fe:P composition. Assuming that the suspended particulate matter Fe:P (0.004–0.005:1; Table 2) is representative of the microbial community integrated biological demand, we derive an atmospheric contribution of ∼0.2–0.4% to the Fe:P_i flux into the mixed layer, with the remaining flux (99.6–99.8%) being driven by nutrient diffusion and mixing at the base of the euphotic zone. This result suggests that interannual variations in the dust deposition rate may have a disproportionate effect on the elemental stoichiometry of the nutrient flux fueling the upper layers of the euphotic zone.

Unfortunately, the biogenic particulate export of Fe is poorly constrained due to the overwhelming lithogenic Fe contribution to the particulate flux (63). In addition, the estimated mean rates of dust-associated soluble Fe deposition at Station ALOHA range broadly, from 0.02 $\mu mol \cdot m^{-2} \cdot d^{-1}$, based on Earth system atmospheric model output (64), to 0.13 $\mu mol \cdot m^{-2} \cdot d^{-1}$, based on in situ aluminum-derived dust deposition rates (65) and considering that Fe accounts for 3.5% of the dust mass with solubility of 5% and 14% for dry and wet deposition, respectively (11). These uncertainties in dust-associated Fe deposition and particulate export fluxes preclude a precise analysis of the coupling between the Fe and P_i biogeochemical cycles at Station ALOHA. Nevertheless, based on the extent of Fe:P stoichiometries observed in representative photoautotrophs found in subtropical oligotrophic regions (Table 2) and the range in dust-associated Fe deposition rates, we estimate that the atmospheric Fe deposition fluxes can account for the net biological uptake of P_i ranging from ∼10 to ∼100 nmol $P_i \cdot L^{-1} \cdot y^{-1}$, averaged over the upper 100 m of the euphotic zone. These values are equivalent to ∼16% and 160% of the mean annual P_i concentration observed at Station ALOHA, further supporting the notion that the observed interannual oscillations of P_i in the upper euphotic zone reflect small changes in the balance between dust deposition rates, driven by large basin-scale atmospheric circulation, and the upward flux of nutrients across the base of the euphotic zone, constrained by the water column stratification.

Climate-Driven Oscillation in Microbial Metabolic P_i Limitation

Over broad spatial and temporal scales, the elemental stoichiometry of ocean and atmospheric nutrient supply relative to that of biological demand defines the identity of the nutrient limiting the ecosystem's carrying capacity (14, 66). For this reason, the uncoupling of nutrient inputs to surface waters through the diffusion and mixing of nutrient-enriched deep waters and from atmospheric sources in vast oligotrophic regions of the ocean may lead to important shifts in microbial diversity and ecosystem structure, without a discernable change in productivity or total biomass (*SI Appendix*, Table S1).

To date, long-term ecosystem shifts in the NPSG associated with large-scale climate variations (23, 67) have been explained primarily as ecosystem-level responses to changes in ocean stratification and advection (68) (Fig. 5). Our observations suggest that, because this oligotrophic pelagic ecosystem is colimited by P_i and Fe, changes in atmospheric dust deposition driven by climate variations in basin-scale atmospheric circulation are an important factor in determining the nutrient that ultimately limits its carrying capacity, as well as the metabolic activity of its microbial assemblage. Furthermore, while small changes in Fe supply may lead to changes in cell physiology, larger sustained changes will affect the ecosystem structure and function (69). Hence, although ocean stratification and advection are important determinants of the pelagic ecosystem structure, our results indicate that the dynamics of atmospheric Fe deposition in this oceanic oligotrophic gyre can also contribute to the regulation of microbial functional diversity with potential cascading effects on new production and CO_2 sequestration (10, 14, 33). Enhancing long-term observational and modeling capabilities that couple ocean and atmosphere biogeochemical dynamics will be critical to further test this hypothesis.

Present climate models reveal that atmospheric pressure gradients over midlatitudes in the Northern Hemisphere will change in response to the warming of the Arctic Ocean (70). Furthermore, secular trends in anthropogenic aerosol emissions rich in soluble Fe and fixed N, as well as in land desertification, may also lead to shifts in nutrient limitation in open ocean oligotrophic ecosystems (54, 71). To develop accurate ecosystem and biogeochemical models that help constrain uncertainties on the temporal evolution of these vast open ocean biomes, there is a need to improve our understanding of how changes in atmospheric pressure gradients and anthropogenic activity will affect the source, transport, and deposition of dust Fe and pollutants into the oligotrophic ocean and, in turn, how long-term shifts in atmospheric deposition will translate to ecosystem structure and function, affecting the biological coupling of energy and elemental cycles.

Methods

Station ALOHA records of inorganic phosphorus (P_i), nitrate + nitrite ($NO_3^- + NO_2^-$), chlorophyll *a* concentrations, primary productivity, temperature, salinity, and water column potential density in the upper 200 m were obtained from the HOT program. The program description, data access, and a full description of methods are publicly available at http://hahana.soest.hawaii.edu/hot/. High-sensitivity analytical techniques were used to determine P_i and $NO_3^- + NO_2^-$ concentrations in the euphotic zone (termed low-level phosphate and low-level nitrogen in the HOT archive). Chlorophyll *a* concentrations were measured by high-performance liquid chromatography. Mean 0- to 45-m P_i concentrations for each HOT cruise between October 1988 and December 2015 were computed (standard collection depths at 5, 25, and 45 m) and a total of 261 time points were splined over the full time record, corresponding to an approximate resolution of one observation every 38 d. Similarly, the mean 0- to 45-m ^{14}C-based primary production rates, $NO_3^- + NO_2^-$, and chlorophyll *a* concentrations, as well as mixed-layer temperature, salinity, density, and the density gradient between the mixed layer and 150 m were computed for each cruise. In addition, because the seasonal cycle is a major contributor to the observed variability of upper water column chlorophyll *a* concentrations, primary productivity, and mixed-layer temperature, salinity, and density at Station ALOHA, all correlation analyses of these variables were based on the residual time series obtained after removing the mean seasonal cycle by subtracting the climatological (1989–2015) monthly mean. The mean drift direction and speed of the surface-tethered sediment traps were computed for each cruise based on the time and position of deployment and recovery.

The analysis of microbial P_i uptake kinetics excludes those assays identified by Björkman et al. (27) as yielding questionable K_m values due to a flat uptake response to P_i loading.

NPGO and PDO monthly values are available from Emanuele Di Lorenzo (http://www.o3d.org/npgo/) and Nathan Mantua (http://research.jisao.washington.edu/pdo/), respectively. SLP data are based on the ERA interim global analysis (72) and were provided by the Asia-Pacific Data Research Center, which is part of the International Pacific Research Center at the University of Hawai'i at Manoa. Monthly Mauna Loa atmospheric aerosol Fe concentrations were calculated from the biweekly records published by Hyslop et al. (59). Hourly wind speed and direction record from 1988 through 2015 were obtained from buoys 51001 and 51101 maintained by the National Data Buoy Center (https://www.ndbc.noaa.gov/). Ocean surface currents, integrated over a 2° × 2° area centered at 23.2°N and 157.2°W for the period 1988 through 2015, were obtained from The Tropical Ocean Surface Currents Analysis Real-time–OSCAR dataset (http://oceanmotion.org/html/resources/oscar.htm).

Because the P_i record displayed the lowest temporal resolution, all other records were splined to match the P_i resolution before cross-correlation analysis. Furthermore, we applied a 10-point Savitzky–Golay smoothing filter (73) to all splined time series to minimize the effects of intraannual variability.

The skill of the hindcast of P_i* based on Eq. **1** and SLP (Fig. 3) was calculated as follows:

$$s = 1 - \frac{\sum_t \left(P_i - P_i^*\right)^2}{\sum_t P_i^2}. \quad [2]$$

The maximum skill score of 0.57 is significant compared with the null hypothesis of forcing by a white Gaussian noise SLP time series. Repeating the fit

with 1,891 white-noise time-series runs as forcing yielded lower skill scores for 99.98% of cases.

Modeled dust aerosol optical depth, atmospheric Fe, and soluble Fe concentration spatial and temporal distributions were derived from the National Science Foundation/Department of Energy (NSF/DOE) CESM/CAM (62, 74), using MERRA reanalysis-based simulations for (1980–2015) and included an intermediate complexity soluble iron scheme (53). This scheme incorporates prognostic dust generation, including soil mineralogy differences (75, 76), and dust; iron and soluble iron are all transported and deposited in the three-dimensional model at $2° \times 2°$ resolution (61). Comparisons to Mauna Loa Fe observations are at the model level corresponding to the height of the observatory (3.4 km), while the PDO correlations were at the surface model level.

ACKNOWLEDGMENTS. This research was funded by the NSF (HOT, OCE-1260164; Center for Microbial Oceanography: Research and Education, EF-0424599), the Gordon and Betty Moore Foundation's Marine Microbiology Initiative (D.M.K.; Grant 3794), the Simons Foundation (Simons Collaboration on Ocean Processes and Ecology Award 329108; D.M.K., A.E.W., and M.J.C.), and the Balzan Foundation (D.M.K.). N.S. was supported by NSF Grant OCE-1357015 and by the Japan Agency for Marine–Earth Science and Technology and International Pacific Research Center Joint Initiative. N.M.M., R.A.S., and D.S.H. acknowledge support from the DOE (DE-SC0006791 and DE-SC0006735), the NSF (AGS-1049033), and high-performance computing from Yellowstone (ark:/85065/d7wd3xhc) provided by the National Center for Atmospheric Research's Computational and Information Systems Laboratory, supported by the NSF. We are indebted to the research staff, as well as to the captains and crews of the various research vessels involved in supporting the HOT effort.

1. R. M. Letelier, D. M. Karl, M. R. Abbott, R. R. Bidigare, Light driven seasonal patterns of chlorophyll and nitrate in the lower euphotic zone of the North Pacific Subtropical Gyre. *Limnol. Oceanogr.* **49**, 508–519 (2004).
2. A. C. Dave, M. S. Lozier, Local stratification control of marine productivity in the subtropical North Pacific. *J. Geophys. Res.* **115**, C12032 (2010).
3. R. T. Letscher, F. Primeau, J. K. Moore, Nutrient budgets in the subtropical ocean gyres dominated by lateral transport. *Nat. Geosci.* **9**, 815–819 (2016).
4. J. H. Martin, R. M. Gordon, Northeast Pacific iron distributions in relation to phytoplankton productivity. *Deep Sea Res. Part I Oceanogr. Res. Pap.* **35**, 177–196 (1988).
5. R. A. Duce, N. W. Tindale, Atmospheric transport of iron and its deposition in the ocean. *Limnol. Oceanogr.* **36**, 1715–1726 (1991).
6. P. W. Boyd, M. J. Ellwood, The biogeochemical cycle of iron in the ocean. *Nat. Geosci.* **3**, 675–682 (2010).
7. D. M. Karl *et al*., Dinitrogen fixation in the world's oceans. *Biogeochemistry* **57**, 47–98 (2002).
8. D. M. Karl Nutrient dynamics in the deep blue sea. *Trends Microbiol.* **10**, 410–418 (2002).
9. J. A. Sohm, E. A. Webb, D. G. Capone, Emerging patterns of marine nitrogen fixation. *Nat. Rev. Microbiol.* **9**, 499–508 (2011).
10. B. A. Ward, S. Dutkiewicz, C. M. Moore, M. J. Follows, Iron, phosphorus, and nitrogen supply ratios define the biogeography of nitrogen fixation. *Limnol. Oceanogr.* **58**, 2059–2075 (2013).
11. M. Martino *et al*., Western Pacific atmospheric nutrient deposition fluxes, their impact on surface ocean productivity. *Global Biogeochem. Cycles* **28**, 712–728 (2014).
12. I. Berman-Frank, A. Quigg, Z. V. Finkel, A. J. Irwin, L. Haramaty, Nitrogen-fixation strategies and Fe requirements in cyanobacteria. *Limnol. Oceanogr.* **52**, 2260–2269 (2007).
13. N. G. Walworth *et al*., Mechanisms of increased *Trichodesmium* fitness under iron and phosphorus co-limitation in the present and future ocean. *Nat. Commun.* **7**, 12081 (2016).
14. R. W. Sterner *et al*., Scale-dependent carbon:nitrogen:phosphorus seston stoichiometry in marine and freshwaters. *Limnol. Oceanogr.* **53**, 1169–1180 (2008).
15. E. D. Galbraith, A. C. Martiny, A simple nutrient-dependence mechanism for predicting the stoichiometry of marine ecosystems. *Proc. Natl. Acad. Sci. U.S.A.* **112**, 8199–8204 (2015).
16. K. K. Cavender-Bares, D. M. Karl, S. W. Chisholm, Nutrient gradients in the western North Atlantic Ocean: Relationship to microbial community structure and comparison to patterns in the Pacific Ocean. *Deep Sea Res. Part I Oceanogr. Res. Pap.* **48**, 2373–2395 (2001).
17. J. Wu, W. Sunda, E. A. Boyle, D. M. Karl, Phosphate depletion in the western North Atlantic Ocean. *Science* **289**, 759–762 (2000).
18. T. Moutin *et al*., Phosphate availability and the ultimate control of new nitrogen input by nitrogen fixation in the tropical Pacific Ocean. *Biogeosciences* **5**, 95–109 (2008).
19. N. M. Mahowald *et al*., Atmospheric iron deposition: Global distribution, variability, and human perturbations. *Annu. Rev. Mar. Sci.* **1**, 245–278 (2009).
20. I. Berman-Frank, J. T. Cullen, Y. Shaked, R. M. Sherrell, P. G. Falkowski, Iron availability, cellular iron quotas, and nitrogen fixation in *Trichodesmium*. *Limnol. Oceanogr.* **46**, 1249–1260 (2001).
21. T. S. Weber, C. Deutsch, Ocean nutrient ratios governed by plankton biogeography. *Nature* **467**, 550–554 (2010).
22. D. M. Karl, Microbially mediated transformations of phosphorus in the sea: New views of an old cycle. *Annu. Rev. Mar. Sci.* **6**, 279–337 (2014).
23. D. M. Karl *et al*., Ecosystem changes in the North Pacific Subtropical Gyre attributed to the 1991–92 El Niño. *Nature* **373**, 230–234 (1995).
24. D. Stammer, S. Park, A. Köl, R. Lukas, F. Santiago-Mandujano, Causes of large-scale hydrographic changes at the Hawaii Ocean Time series Station. *J. Phys. Oceanogr.* **38**, 1931–1948 (2008).
25. D. M. Karl, M. J. Church, Ecosystem structure and dynamics in the North Pacific Subtropical Gyre: New views of an old ocean. *Ecosystems (N. Y.)* **20**, 433–457 (2017).
26. E. Di Lorenzo *et al*., North Pacific Gyre Oscillation links ocean climate and ecosystem change. *Geophys. Res. Lett.* **35**, L08607 (2008).
27. K. Björkman, S. Duhamel, D. M. Karl, Microbial group specific uptake kinetics of inorganic phosphate and adenosine-5′-triphosphate (ATP) in the North Pacific Subtropical Gyre. *Front. Microbiol.* **3**, 189 (2012).
28. K. S. Watkins-Brandt *et al*., Addition of inorganic or organic phosphorus enhances nitrogen and carbon fixation in the oligotrophic North Pacific. *Mar. Ecol. Prog. Ser.* **432**, 17–29 (2011).
29. M. R. Gradoville, A. E. White, D. Böttjer, M. J. Church, R. M. Letelier, Diversity trumps acidification: Lack of evidence for carbon dioxide enhancement of *Trichodesmium* community nitrogen fixation at Station ALOHA. *Limnol. Oceanogr.* **59**, 645–659 (2014).
30. M. N. W. Grabowski, M. J. Church, D. M. Karl, Nitrogen fixation and controls at Stn ALOHA. *Aquat. Microb. Ecol.* **52**, 175–183 (2008).
31. D. M. Karl *et al*., Ecological nitrogen-to phosphorus stoichiometry at Station ALOHA. *Deep Sea Res. Part II Top. Stud. Oceanogr.* **48**, 1529–1566 (2001).
32. L. J. Beversdorf, A. E. White, K. M. Björkman, R. M. Letelier, D. M. Karl, Phosphonate metabolism of *Trichodesmium* IMS101 and the production of greenhouse gases. *Limnol. Oceanogr.* **55**, 1768–1778 (2010).
33. D. M. Karl, R. R. Bidigare, R. M. Letelier, Long-term changes in plankton community structure and productivity in the North Pacific Subtropical Gyre: The domain shift hypothesis. *Deep Sea Res. Part II Top. Stud. Oceanogr.* **48**, 1449–1470 (2001).
34. N. J. Mantua, S. R. Hare, Y. Zhang, J. M. Wallace, R. C. Francis, A Pacific interdecadal climate oscillation with impacts on salmon production. *Bull. Am. Meteorol. Soc.* **78**, 1069–1079 (1997).
35. N. Schneider, B. D. Cornuelle, The forcing of the Pacific decadal oscillation. *J. Clim.* **18**, 4355–4373 (2005).
36. T. Toyoda *et al*., Inter-annual-decadal variability of wintertime mixed layer depths in the North Pacific detected by an ensemble of ocean syntheses. *Clim. Dyn.* **49**, 891–907 (2015).
37. K. Chhak, E. Di Lorenzo, P. Cummins, N. Schneider, Forcing of low-frequency ocean variability in the Northeast Pacific. *J. Clim.* **22**, 1255–1276 (2009).
38. J. Rogers, The North Pacific Oscillation. *Int. J. Climatol.* **1**, 39–57 (1981).
39. L. I. Ceballos, E. Di Lorenzo, C. D. Hoyos, N. Schneider, B. Taguchi, North Pacific Gyre Oscillation synchronizes climate fluctuations in the eastern and western boundary systems. *J. Clim.* **22**, 5163–5174 (2009).
40. E. Di Lorenzo *et al*., Nutrient and salinity decadal variations in the central and eastern North Pacific. *Geophys. Res. Lett.* **33**, L14601 (2009).
41. F. Bonjean, G. S. E. Lagerloef, Diagnostic model and analysis of the surface currents in the tropical Pacific Ocean. *J. Phys. Oceanogr.* **32**, 2938–2954 (2002).
42. E. Post, "Time lags in terrestrial and marine environments" in *Marine Ecosystems and Climate Variation: The North Atlantic: A Comparative Perspective*, N. C. Stenseth, G. Ottersen, J. W. Hurrell, A. Belgrano, Eds. (Oxford University Press Inc., New York, 2004), pp. 165–168.
43. C. A. Neal *et al*., The 2018 rift eruption and summit collapse of Kilauea Volcano. *Science* **363**, 367–374 (2019).
44. D. M. Karl, G. Tien, Temporal variability in dissolved phosphorus concentrations in the subtropical North Pacific Ocean. *Mar. Chem.* **56**, 77–96 (1997).
45. N. Olgun *et al*., Surface ocean iron fertilization: The role of airborne volcanic ash from subduction zone and hot spot volcanoes and related iron fluxes into the Pacific Ocean. *Global Biogeochem. Cycles* **25**, GB4001 (2011).
46. F. Sansone *et al*., Geochemistry of atmospheric aerosols generated from lava-seawater interactions. *Geophys. Res. Lett.* **29**, 1335 (2002).
47. A. T. Hollingshead, S. Businger, R. Draxler, J. Porter, D. Stevens, Dispersion modeling of the Kilauea plume. *Boundary-Layer Meteorol.* **108**, 121–144 (2003).
48. H. K. Fröllje *et al*., Hawaiian imprint of dissolved Nd and Ra isotopes and rare earth elements in the central North Pacific: Local survey and seasonal variability. *Geochim. Cosmochim. Acta* **189**, 110–131 (2016).
49. M. Newman, G. P. Compo, M. A. Alexander, ENSO-forced variability of the Pacific decadal oscillation. *J. Clim.* **16**, 3853–3857 (2003).
50. J. T. Merrill, M. Uematsu, R. Bleck, Meteorological analysis of long range transport of mineral aerosols over the North Pacific. *J. Geophys. Res. Atmos.* **94**, 8584–8598 (1989).
51. T. L. Zhao *et al*., A simulated climatology of Asian dust aerosol and its trans-Pacific transport. Part I: Mean climate and validation. *J. Clim.* **19**, 88–103 (2006).
52. C. Luo *et al*., Combustion iron distribution and deposition. *Global Biogeochem. Cycles* **22**, GB1012 (2008).
53. H. Matsui *et al*., Anthropogenic combustion iron as a complex climate forcer. *Nat. Commun.* **9**, 1593 (2018).
54. S. L. Gong *et al*., A simulated climatology of Asian dust aerosol and its trans-Pacific transport. Part II: Inter-annual variability and climate connections. *J. Clim.* **19**, 104–122 (2006).

55. J. N. Fitzsimmons *et al*., Daily to decadal variability of size-fractionated iron and iron-binding ligands at the Hawaii Ocean Time-series Station ALOHA. *Geochim. Cosmochim. Acta* **171**, 303–324 (2015).
56. J. M. Prospero, "Mineral aerosol transport to the North Atlantic and North Pacific: The impact of African and Asian sources" in *The Long-Range Atmospheric Transport of Natural and Contaminant Substances*, A. H. Knap, Ed. (Kluwer, Boston, Mass., 1990), pp. 59–86.
57. K. S. Johnson *et al*., Surface ocean-lower atmosphere interactions in the Northeast Pacific Ocean Gyre: Aerosols, iron, and the ecosystem response. *Global Biogeochem. Cycles* **17**, 1063 (2003).
58. D. M. Karl, R. M. Letelier, Nitrogen fixation-enhanced carbon sequestration in low nitrate, low chlorophyll seascapes. *Mar. Ecol. Prog. Ser.* **364**, 257–268 (2008).
59. N. P. Hyslop, K. Trzepla, C. D. Wallis, A. K. Matzoll, W. H. White, Technical note: A 23-year record of twice-weekly aerosol composition measurements at Mauna Loa Observatory. *Atmos. Environ.* **80**, 259–263 (2013).
60. S. Albani *et al*., Improved dust representation in the Community Atmosphere Model. *J. Adv. Model. Earth Syst.* **6**, 541–570 (2014).
61. R. A. Scanza *et al*., Atmospheric processing of iron in mineral and combustion aerosols: Development of an intermediate-complexity mechanism suitable for Earth system models. *Atmos. Chem. Phys.* **18**, 14175–14196 (2018).
62. M. B. Smith *et al*., Sensitivity of the inter-annual variability of mineral aerosol simulations to meteorological forcing dataset. *Atmos. Chem. Phys.* **17**, 3253–3278 (2016).
63. C. H. Lamborg, K. O. Buesseler, P. J. Lam, Sinking flux of minor and trace elements in the North Pacific Ocean measured during the VERTIGO program. *Deep Sea Res. Part II Top. Stud. Oceanogr.* **55**, 1564–1577 (2008).
64. C. Chien *et al*., Effects of African dust deposition on phytoplankton in the western tropical Atlantic Ocean off Barbados. *Global Biogeochem. Cycles* **30**, 716–734 (2016).
65. C. I. Measures, M. T. Brown, S. Vink, Dust deposition to the surface waters of the western and central North Pacific inferred from surface water dissolved aluminum concentrations. *Geochem Geophys Geosys* **6**, Q09M03 (2005).
66. C. M. Moore *et al*., Processes and patterns of oceanic nutrient limitation. *Nat. Geosci.* **6**, 701–710 (2013).
67. R. R. Bidigare *et al*., Subtropical ocean ecosystem structure changes forced by North Pacific climate variations. *J. Plankton Res.* **31**, 1131–1139 (2009).
68. A. J. Miller, F. Chai, S. Chiba, J. R. Moisan, D. J. Neilson, Decadal-scale climate driven ecosystem interactions in the North Pacific ocean. *J. Oceanogr.* **60**, 163–188 (2004).
69. D. A. Hutchins, P. W. Boyd, Marine phytoplankton and the changing iron cycle. *Nat. Clim. Chang.* **6**, 1071–1079 (2016).
70. J. A. Francis, J. S. Vavrus, Evidence linking Arctic amplification to extreme weather in mid-latitudes. *Geophys. Res. Lett.* **39**, L06801 (2012).
71. I. N. Kim *et al*., Chemical oceanography. Increasing anthropogenic nitrogen in the North Pacific Ocean. *Science* **346**, 1102–1106 (2014).
72. D. P. Dee *et al*., The ERA-interim reanalysis: Configuration and performance of the data assimilation system. *Q. J. R. Meteorol. Soc.* **137**, 553–597 (2011).
73. A. Stavitzky, M. J. E. Golay, Smoothing and differentiation of data by simplified least squares procedures. *Anal. Chem.* **36**, 1627–1639 (1964).
74. J. W. Hurrell *et al*., The community earth system model: A framework for collaborative research. *Bull. Am. Meteorol. Soc.* **94**, 1339–1360 (2013).
75. Y. Zang *et al*., Modeling the global emission, transport and deposition of trace elements associated with mineral dust. *Biogeosciences* **12**, 5771–5792 (2015).
76. R. Scanza *et al*., Modeling dust as component minerals in the Community Atmosphere Model: Development of framework and impact on radiative transfer. *Atmos. Chem. Phys.* **15**, 537–561 (2015).
77. M. T. Brown, W. M. Landing, C. I. Measures, Dissolved and particulate Fe in the western and central North Pacific: Results from the 2002 IOC cruise. *Geochem. Geophys. Geosyst.* **6**, Q10001 (2005).
78. E. A. Boyle, B. A. Bergquist, R. A. Kayser, N. Mahowald, Iron, manganese, and lead at Hawaii Ocean Time-series station ALOHA: Temporal variability and an intermediate water hydrothermal plume. *Geochim. Geophys. Acta* **69**, 933–952 (2005).
79. H. Furutani, A. Meguro, H. Iguchi, M. Uematsu, Geographical distribution and sources of phosphorus in atmospheric aerosol over the North Pacific Ocean. *Geophys. Res. Lett.* **37**, L03805 (2010).
80. S. Bertilsson, O. Berglund, D. M. Karl, S. W. Chisholm, Elemental composition of marine *Prochlorococcus*: Implications for the ecological stoichiometry of the sea. *Limnol. Oceanogr.* **48**, 1721–1731 (2003).
81. I. Kudo, P. J. Harrison, Effect of iron nutrition on the marine *Synechococcus* grown on different N sources and irradiances. *J. Phycol.* **33**, 232–240 (1997).
82. B. S. Twining, D. Nuñez-Milland, S. Vogt, R. S. Jonson, P. N. Sedwick, Variations in *Synechococcus* cell quotas of phosphorus, sulfur, manganese, iron, nickel, and zinc within mesoscale eddies in the Sargasso Sea. *Limnol. Oceanogr.* **55**, 492–506 (2010).
83. D. M. Shire, A. B. Kutska, Luxury uptake, iron storage and ferritin abundance in *Prochlorococcus marinus* (Synechoccales) strain MED4. *Phycologia* **54**, 398–406 (2015).
84. N. M. Price, The elemental stoichiometry and composition of an iron-limited diatom. *Limnol. Oceanogr.* **50**, 1159–1171 (2005).
85. F. X. Fu *et al*., Interactions between changing pCO_2, N_2 fixation, and Fe limitation in the marine unicellular cyanobacterium *Crocosphaera*. *Limnol. Oceanogr.* **53**, 2472–2484 (2008).
86. A. B. Kutska, S. Sañudo-Wilhelmy, E. J. Carpenter, Iron requirements for dinitrogen- and ammonium-supported growth in cultures of *Trichodesmium* (IMS 101): Comparison with nitrogen fixation rates and iron:carbon ratios of field populations. *Limnol. Oceanogr.* **48**, 1869–1884 (2003).
87. J. Nuester, S. Vogt, M. Newville, A. B. Kustka, B. S. Twining, The unique biogeochemical signature of the marine diazotroph *Trichodesmium*. *Front. Microbiol.* **3**, 150–164 (2012).
88. J. Kuss, K. Kremling, Spatial variability of particle associated trace elements in near-surface waters of the North Atlantic (30°N/60°W to 60°N/2°W), derived by large volume sampling. *Mar. Chem.* **68**, 71–86 (1999).
89. R. Collier, J. Edmond, The trace element geochemistry of marine biogenic particulate matter. *Prog. Oceanogr.* **13**, 113–199 (1984).
90. J. H. Martin, K. W. Bruland, W. W. Broenkow, "Cadmium transport in the California current" in *Marine Polutant Transfer*, H. L. Windom, R. Duce, Eds. (D.C. Heath, Lexington, MA, 1976), pp. 159–184.
91. B. S. Twining *et al*., Metal quotas of phytoplankton in the equatorial Pacific Ocean. *Deep Sea Res. Part II Top. Stud. Oceanogr.* **58**, 325–341 (2011).